Stokes Flow Heat Transfer In An Annular, Rotating Heat Exchanger

E. Saatdjian, A.J.S. Rodrigo, J.P.B. Mota

Accepted Manuscript

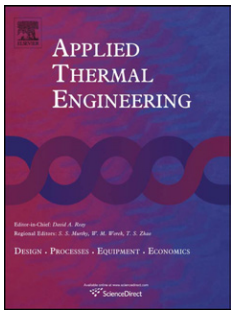

Title: Stokes Flow Heat Transfer In An Annular, Rotating Heat Exchanger

Authors: E. Saatdjian, A.J.S. Rodrigo, J.P.B. Mota

PII: S1359-4311(11)00061-5

DOI: 10.1016/j.applthermaleng.2011.01.037

Reference: ATE 3401

To appear in: *Applied Thermal Engineering*

Received Date: 19 August 2010

Revised Date: 19 January 2011

Accepted Date: 21 January 2011

Please cite this article as: E. Saatdjian, A.J.S. Rodrigo, J.P.B. Mota. Stokes Flow Heat Transfer In An Annular, Rotating Heat Exchanger, Applied Thermal Engineering (2011), doi: 10.1016/j.applthermaleng.2011.01.037

Stokes Flow Heat Transfer in an Annular, Rotating Heat Exchanger

E. Saatdjian,[1] A.J.S. Rodrigo,[2] J.P.B. Mota,[2,*]

[1]LEMTA GDR 681: Chaos Lagrangien 3-D, 2 ave. de la forêt de Haye, BP 160, 54504 Vandœuvre Cédex, France

[2]Requimte/CQFB, Departamento de Química, Faculdade de Ciências e Tecnologia, Universidade Nova de Lisboa, 2829-516 Caparica, Portugal

[*]Corresponding author; Tel.: (351)21 2948385; fax: (351)21 2948550; e-mail: pmota@dq.fct.unl.pt

Keywords: Stokes flows, chaotic advection, heat transfer, mixing, annular rotating heat exchanger

Abstract

The heat transfer rate into highly viscous, low thermal-conductivity fluids can be enhanced significantly by chaotic advection in three-dimensional flows dominated by viscous forces. The physical effect of chaotic advection is to render the cross-sectional temperature field uniform, thus increasing both the wall temperature gradient and the heat flux into the fluid. A method of analysis for one such flow—the flow in the eccentric, annular, rotating heat exchanger—

and a procedure to determine the best heat transfer conditions, namely the optimal values of the eccentricity ratio and time-periodic rotating protocol, are discussed. It is shown that in continuous flows, such as the one under consideration, there exists an optimum frequency of the rotation protocol for which the heat transfer rate is a maximum.

1 Introduction

The efficient heating of high viscosity liquids with a low thermal conductivity is a major engineering problem today due to the increase in the price of energy and also due to a public awareness against processes that waste energy and produce significant amounts of gases, such as carbon dioxide, that are responsible for climate change. The production of cement is one industry sector that is in dire need for improvement since its efficiency is very low. For the production of cement it is necessary to heat oil in a continuous process and this is generally done under turbulent flow conditions and in equipment that is not suitable for highly viscous fluids—the type of fluids whose properties are those considered here.

An appropriate apparatus for heating these high Prandtl number fluids under laminar flow conditions, which is the recommended flow regime for highly viscous fluids since otherwise the pressure drop will be quite large and the energy consumption will be very high, is the annular heat exchanger. In this apparatus the fluid flows in the annular region between two concentric cylinders. The advantage of this apparatus—and it is a major one—is that heat can be introduced into the fluid via both the inner and outer boundaries.

Under laminar flow conditions, it is possible to solve the flow and energy equations analytically and to determine the thermal performance of this apparatus. This has been done by

Kays and co-workers at Stanford University [1]; their results are given in tabular form and for different types of boundary conditions on both walls by Shah and London [2]. One can also find in this last reference analytical and numerical solutions to laminar flow problems in similar geometries such as the eccentric annular region or a confocal elliptic annular region.

This efficient system can be further improved if the two cylinders are allowed to rotate at low angular velocities so that the energy consumption is not too high. If the cylinders are in an eccentric position and if one cylinder is allowed to turn at a periodic angular velocity while the other turns at constant speed, it is possible, under certain conditions, to obtain chaotic streaklines very similar to those occurring in turbulent flows. Pictures of experiments where chaotic streaklines appear in the geometry considered here, but also in the partitioned pipe mixer, were taken by Kusch and Ottino [3]. However these authors have not provided a theoretical analysis and have not explained why the flow becomes regular when the average axial velocity is increased. Chaotic advection in flows dominated by viscous forces can occur in two-dimensional periodic flows, such as the journal bearing flow, and in either spatially periodic [4, 5, 6] or time periodic 3-D flows.

In this paper the eccentric, annular, rotating heat exchanger is analyzed for oscillatory flow at low Strouhal number driven by the counter-rotation of the inner cylinder with a time-periodic angular velocity. When the two cylinders turn at constant velocity, the three velocity components can be determined analytically by solving the Stokes equations. If one cylinder is turned with a periodic angular velocity at a small Strouhal number, one can assume that the velocity profile is given by the analytical solution for steady cylinder rotation calculated at the instantaneous angular velocity ratio. The energy equation is then solved numerically

for adiabatic operation of the heat exchanger to determine the best conditions, namely the eccentricity ratio and modulation frequency, leading to a maximum heat transfer rate from the cylinders to the fluid. It is shown that there is a connection between the operating regime that yields optimal thermal performance and the advection properties of the flow.

2 Flow (3-D) between two eccentric, rotating cylinders

Let us first consider viscous fluid flow between two eccentric cylinders that are rotating at constant angular velocities Ω_1 and Ω_2. The radii of the inner and outer cylinders are R_1 and R_2, respectively, the distance between the centers of the two cylinders is labeled e, and the axial length of both cylinders is L. A sketch of the cross section and a view of the complete apparatus are shown in Fig. 1. The cross-sectional geometry is completely defined by two dimensionless parameters: the clearance ratio, R_2/R_1, and the eccentricity ratio, $\epsilon = e/(R_2 - R_1)$.

The analytical solution for this flow can be obtained by first solving the cross-sectional components of the equations of motion (journal bearing flow) and then solving the axial velocity component of the Stokes equations for pressure-driven axial flow in the eccentric, cylindrical annulus. An appropriate coordinate system for this geometry are the bipolar cylindrical coordinates $[\alpha, \beta, z]$, defined by the following transformations from Cartesian coordinates $[x, y, z]$:

$$x = -\frac{a \sinh \alpha}{\cosh \alpha - \cos \beta}, \quad y = \frac{a \sin \beta}{\cosh \alpha - \cos \beta}, \quad z = z, \tag{1}$$

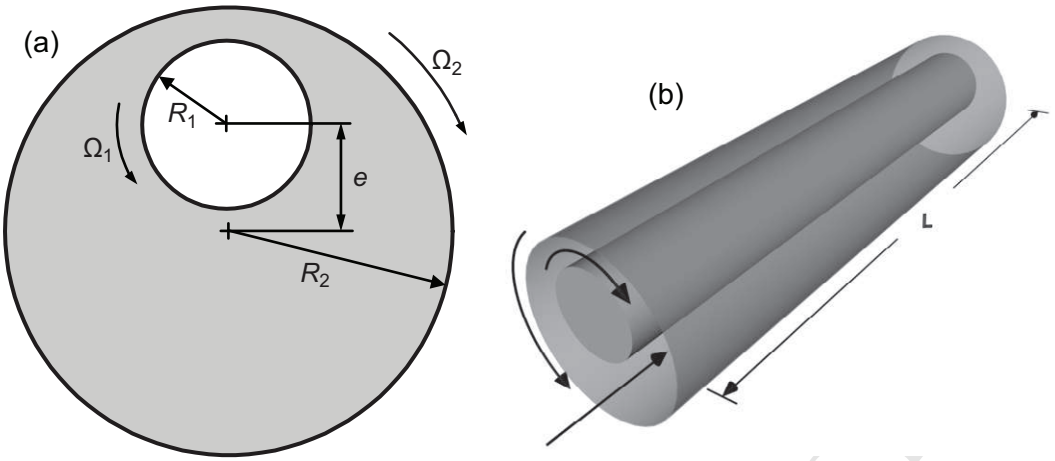

Figure 1: (a) Cross section of the eccentric, rotating, annular heat exchanger and (b) view of the whole apparatus.

---

where

$$a = \frac{R_2 - R_1}{2\epsilon}\left[\left(\frac{R_1 + R_2}{R_2 - R_1} - \epsilon^2\right)^2 - \left(\frac{2R_1\epsilon}{R_2 - R_1}\right)^2\right]^{1/2}. \tag{2}$$

This coordinate system is orthogonal; the scale factors are

$$h_\alpha = h_\beta = h = \frac{a}{\cosh\alpha - \cos\beta}, \quad h_z = 1. \tag{3}$$

In bipolar cylindrical coordinates the inner and outer cylinders correspond to surfaces of constant α; the boundary values, α_1 and α_2, can be determined from the following identities:

$$\alpha_1 = \operatorname{arcsinh}(-a/R_1), \quad \alpha_2 = \operatorname{arcsinh}(-a/R_2). \tag{4}$$

Other coordinate systems have been used to solve this same problem. Wannier [7] used a mixed nonorthogonal, Cartesian–cylindrical coordinate system, whereas DiPrima and Stuart [8] used a modified bipolar coordinate system. Although the bipolar cylindrical coordinates used in the present work do not convert to cylindrical coordinates as the eccentricity tends

revised

towards zero, they are probably the most adequate because the mathematical expressions are simpler than in the other coordinate systems.

When the two cylinders rotate at constant velocity, and assuming that inertial effects are negligible, the equations of motion for the cross-sectional flow can be written as

$$\frac{\partial^2\omega}{\partial\alpha^2}+\frac{\partial^2\omega}{\partial\beta^2}=0, \quad -h^2\omega=\frac{\partial^2\psi}{\partial\alpha^2}+\frac{\partial^2\psi}{\partial\beta^2}, \tag{5}$$

where ω is the axial component of the vorticity vector and ψ is the stream function defined as

$$hV_\beta=-\frac{\partial\psi}{\partial\alpha}, \quad hV_\alpha=\frac{\partial\psi}{\partial\beta}. \tag{6}$$

Here, V_α and V_β are the two cross-sectional components of the velocity vector.

The analytical solution to the above equations with the expressions of all the constants is quite long and is not fully reproduced here; it is given by Ballal and Rivlin [9]. In short, the solution can be written as

$$\psi=h\left[F_0(\alpha)+F_1(\alpha)\cos\beta\right], \tag{7}$$

$$F_0(\alpha)=(A_0+C_0\alpha)\cosh\alpha+(B_0+D_0\alpha)\sinh\alpha, \tag{8}$$

$$F_1(\alpha)=A_1\cosh 2\alpha+B_1\sinh 2\alpha A_1+C_1\alpha+D_1, \tag{9}$$

where the A_i, B_i, C_i, and D_i are constants determined from the boundary conditions. These are the prescribed angular velocities of both cylinders (Ω_1 and Ω_2) and the no-slip boundary conditions.

The axial velocity component, V_z, is obtained by solving the axial component of the equation of motion,

$$h^2\frac{dP}{dz}=\mu\left(\frac{\partial^2V_z}{\partial\alpha^2}+\frac{\partial^2V_z}{\partial\beta^2}\right), \tag{10}$$

where μ is the fluid viscosity and dP/dz is the pressure drop per unit axial length of the heat exchanger. The analytical solution to this problem is given in Snyder and Goldstein [10]; the axial velocity is

$$V_z = -\frac{a^2}{\mu}\frac{dP}{dz}\left(F + E\alpha - \frac{\coth\alpha}{2} + \sum_{n=1}^{\infty}\left[A_n e^{n\alpha} + (B_n - \coth\alpha)e^{-n\alpha}\right]\cos n\beta\right), \tag{11}$$

where

$$F = \frac{\alpha_1 \coth\alpha_2 - \alpha_2 \coth\alpha_1}{2(\alpha_1 - \alpha_2)}, \quad E = \frac{\coth\alpha_1 - \coth\alpha_2}{2(\alpha_1 - \alpha_2)}, \tag{12}$$

$$A_n = \frac{\coth\alpha_1 - \coth\alpha_2}{\exp(2n\alpha_1) - \exp(2n\alpha_2)} \quad B_n = \frac{\exp(2n\alpha_1)\coth\alpha_2 - \exp(2n\alpha_2)\coth\alpha_1}{\exp(2n\alpha_1) - \exp(2n\alpha_2)}. \tag{13}$$

The average axial velocity over the cross section $A = \pi(R_2^2 - R_1^2)$ of the eccentric annular region, $\langle V_z\rangle = A^{-1}\iint_A V_z\, dA$, is defined in terms of bipolar coordinates as

$$\langle V_z\rangle = \frac{2a^2}{\pi(R_2^2 - R_1^2)}\int_{\alpha_1}^{\alpha_2}\int_0^{\pi}\frac{V_z}{(\cosh\alpha - \cos\beta)^2}\, d\alpha\, d\beta. \tag{14}$$

To determine $\langle V_z\rangle$ for a given geometry, Eq. (11) is substituted into Eq. (14) and the latter is integrated numerically; this gives

$$\langle V_z\rangle = -K\frac{a^2}{\mu}\frac{dP}{dz}, \tag{15}$$

where K is a constant that depends on R_2/R_1 and ϵ.

The three velocity components for the case where both cylinders are turning at constant speed have been determined analytically by first solving for the two cross-sectional components, V_α and V_β, and then for the axial component V_z; furthermore all three velocity components are independent of the axial coordinate z. For these reasons, this flow is not strictly 3-D but really is 2.5-D.

When both cylinders turn at constant speed, the streaklines are helicoidal as shown experimentally by Kusch and Ottino [3]. In order to promote chaotic advection in this flow, at least one of the cylinders must turn at a time-varying angular velocity. In what follows, it is assumed that the outer cylinder turns at a constant angular velocity Ω_2, whereas the inner cylinder is allowed to rotate in the opposite direction (counter-rotation) with a time-periodic angular velocity:

$$\Omega_1 = \overline{\Omega}_1(1 + \delta \sin \omega t), \quad \overline{\Omega}_1 \cdot \Omega_2 < 0, \tag{16}$$

where δ and ω are the amplitude and frequency of the inner-cylinder modulation.

The analytical solution of the cross-sectional velocity components, Eqs. (7)–(9), is valid only if the cylinders rotate at constant angular velocities and if the inertial terms are negligible. However, if the modulation frequency ω is small then the Strouhal number $\mathrm{Sr} = \omega L_{\mathrm{ref}}/V_{\mathrm{ref}}$, where L_{ref} and V_{ref} are characteristic length and velocity scales for the cross-sectional flow, is also small. This assumption allows us to consider the flow to be quasi-static and the velocity profile to be given by the analytical solution for steady rotation at the instantaneous angular velocity ratio. This can be written mathematically as

$$\mathbf{V}(\alpha, \beta, t) \approx \mathbf{V}(\alpha, \beta)|_{\Omega_1(t), \Omega_2}. \tag{17}$$

The flow is also quasi-static if $\delta \ll 1$, but this is not the case under consideration here. A complete discussion of this assumption and of the Strouhal number is given later on.

3 Heat transfer in the rotating, eccentric, annular heat exchanger

Now that the velocity profile in the eccentric, rotating, annular heat exchanger is known analytically, the temperature distribution in the heat exchanger can be determined by solving numerically the conservation of energy equation for an incompressible, Newtonian fluid neglecting viscous dissipation:

$$\frac{\partial T}{\partial t} + \mathbf{V} \cdot \nabla T = \eta \nabla^2 T, \tag{18}$$

where $\eta = k/\rho c_p$ is the thermal diffusivity of the fluid; k, ρ, and c_p are, respectively, the thermal conductivity, the density, and the heat capacity of the fluid.

As mentioned above, for the concentric annular heat exchanger without any rotation, Kays [1] obtained solutions to four different problems corresponding to different boundary conditions. From these solutions an internal and an external Nusselt number can be defined.

Here, the purpose is to determine the geometry and the way the cylinders have to turn in order to maximize the heat transfer rate to the fluid. Let us examine in detail the heat transfer characteristics and the possible ways of increasing the heat transfer rate into the fluid in this system. Under laminar flow conditions and when the two cylinders are motionless, in either a concentric or eccentric position, the velocity profile is one-dimensional in the axial direction; Nusselt numbers for both the fully developed temperature profile and for the developing profile were calculated by Shah and London [2].

For the concentric case, if one or both cylinders are allowed to rotate at constant speed and assuming that laminar flow prevails, there will be no heat transfer enhancement because

the heat flux is in the radial direction and the radial velocity component and the advection terms $\mathbf{V} \cdot \nabla T = 0$ are both zero.

When the cylinders are in an eccentric position and rotating at constant speed, the heat transfer rate enhancement is due to the velocity component in the heat flux direction; the temperature gradient and thus the heat transfer rate at both walls increases. In the journal bearing flow this same phenomenon occurs, it is due to the recirculation region as shown by Ghosh et al. [11]. In the eccentric case, when both cylinders turn with one of them turning at a periodic angular velocity, there will be a further heat transfer rate enhancement due to chaotic advection. This phenomenon occurs in the flow considered here as well as in the journal bearing flow. Chaotic advection also tends to homogenize the cross sectional temperature field so that the temperature gradient at the walls and the heat transfer rate into the fluid both increase.

For this reason the following numerical experiment was devised: the heat exchanger is assumed adiabatic, i.e., no heat is exchanged through the cylindrical walls, and the fluid entering the heat exchanger has a nonuniform temperature distribution. For simplicity, the inlet temperature field, $T(\alpha, \beta, z = 0)$, is taken to be linear in the α coordinate, which is the main direction for cross-sectional heat transfer, such that

$$T(\alpha, \beta, 0) = T_1 + \frac{T_2 - T_1}{\alpha_2 - \alpha_1} (\alpha - \alpha_1), \tag{19}$$

where T_1 and T_2 are the extreme values of the temperature distribution.

Now, since the heat exchanger is adiabatic, the best velocity protocol and the best geometry will be the ones that give the most uniform outlet temperature distribution—ideally, the fluid will exit the heat exchanger at a constant temperature.

In mathematical terms, the mixed-mean temperature at axial position z in the heat exchanger and time t, i.e., the average temperature over the cross section at z if that infinitesimal slice of fluid is put into an adiabatic cup at time t, is defined as

$$\langle T\rangle(z,t) = \frac{1}{A\,\langle V_z\rangle}\iint_A V_z(\alpha,\beta)\,T(\alpha,\beta,z;t)\,dA. \tag{20}$$

The standard deviation of the cross-sectional temperature field, $\sigma'(z,t)$, at axial position z and time t is obtained by calculating

$$[\sigma'(z,t)]^2 = \frac{1}{A\,\langle V_z\rangle}\iint_A V_z(\alpha,\beta)\,[T(\alpha,\beta,z;t) - \langle T\rangle(z,t)]^2\,dA. \tag{21}$$

To make the results less dependent on the shape of the chosen inlet temperature distribution, $\sigma'(z,t)$ is normalized with respect to its inlet value:

$$\sigma(z,t) = \sigma'(z,t)/\sigma'(0,t). \tag{22}$$

Since the velocity distribution is time-periodic because of the inner cylinder modulation, the exit standard deviation will also be time-periodic after the influence of the initial conditions vanishes. Therefore, the average value of the standard deviation over a period of modulation,

$$\overline{\sigma}(z,t) = \frac{\omega}{2\pi}\int_t^{t+2\pi/\omega}\sigma(z,t)\,dt \tag{23}$$

will be time invariant after a sufficiently long period of time. We denote by $\overline{\sigma}^{\infty}(z)$ the axial $\overline{\sigma}$-profile when this steady-periodic regime is established; the value for the outlet cross section of the heat exchanger is $\overline{\sigma}^{\infty}(L)$. The best heat transfer conditions, namely the optimal values of the eccentricity ratio and time-periodic rotating protocol, are those that minimize the value of $\overline{\sigma}^{\infty}(L)$.

The numerical solution of the energy equation in bipolar cylindrical coordinates, with the velocity field determined by the analytical solution, was obtained using OpenFOAM®, an open source computational-fluid-dynamics (CFD) toolbox [12]. It is worth noting that the existence of an analytical solution for the velocity field reduces significantly the CPU time required to compute the numerical solution.

The results given below were obtained on a structured grid with $50 \times 80 \times 60$ (α, β, z) points covering the eccentric, cylindrical annulus of the heat exchanger. The diffusive term in Eq. (18) was discretized using second-order central differences, whereas the advection term was approximated by the second-order QUICK scheme [13] combined with the van Leer's symmetric flux limiter [14] to reduce numerical diffusion and spurious oscillations in the computed solution.

Results and Discussion

As in [15, 16], two dimensionless control parameters, N_T and N_P, are first defined. The former parameter gives the number of rotations that the outer cylinder makes per average residence time in the annular heat exchanger:

$$N_T = \frac{\Omega_2 \tau}{2\pi}, \tag{24}$$

where $\tau = L/\langle V_z \rangle$ is the average residence time of a fluid particle in the apparatus. The second parameter, N_P, is related to the number of *periods* the inner cylinder makes per average residence time:

$$N_P = \frac{\omega \tau}{2\pi}. \tag{25}$$

Previous work [17] on chaotic advection in the 2-D flow between two eccentric cylinders ($V_z = 0$) showed that the amplitude of the modulation must be chosen as large as possible, as long as the Stokes flow conditions are maintained. This way, the instantaneous hyperbolic fixed point that exists in the region of minimum gap is periodically displaced from the vicinity of one cylinder to the vicinity of the other. The periodic forcing allows exchange of fluid between the three regions separated by the two streamlines stagnating on the hyperbolic point. For this reason, in the present work δ is fixed at a large value ($\delta = 0.9$). revised

In all cases analyzed the heat exchanger is operated under Stokes flow conditions. The axial and cross-sectional Péclet numbers, $\mathrm{Pe}_z = \langle V_z \rangle L/\eta$ and $\mathrm{Pe}_\Omega = |\Omega_2| R_2 (R_2 - R_1)/\eta$, are both fixed at 5000. Let us now reconsider the effects of time periodicity in this apparatus. For the fluid to respond quasi-statically to the modulation of the inner boundary, the Strouhal number must be small, $\mathrm{Sr} < 1$. If the characteristic length is taken equal to the annular gap spacing, $L_{\mathrm{ref}} = R_2 - R_1$, and the characteristic velocity taken equal to the average value for the oscillatory cylinder, $V_{\mathrm{ref}} = R_1 \overline{\Omega}_1$, then $\mathrm{Sr} = (R_2/R_1 - 1)(|\Omega_2|/\overline{\Omega}_1)(N_P/N_T)$. For $R_2/R_1 = 2$, $|\Omega_2|/\overline{\Omega}_1 = 1/2$, and $N_T = 30$ used in our calculations, we get $\mathrm{Sr} = N_P/60$. Thus, to keep $\mathrm{Sr} < 1$ implies $N_P < 60$. Although the calculations were carried out up to $N_P = 64$, we shall see that the interesting results are obtained for $N_P < 40$. Therefore, the underlying assumption of quasi-static flow seems to be a reasonable one and is not expected to compromise the physical meaningfulness of the results.

The influence of the modulation frequency is first examined for a specific geometry, defined by a clearance ratio $R_2/R_1 = 2$ and an eccentricity ratio $\epsilon = 0.5$. Figure 2 shows the normalized standard deviation of the outlet temperature field as a function of N_P for a fixed

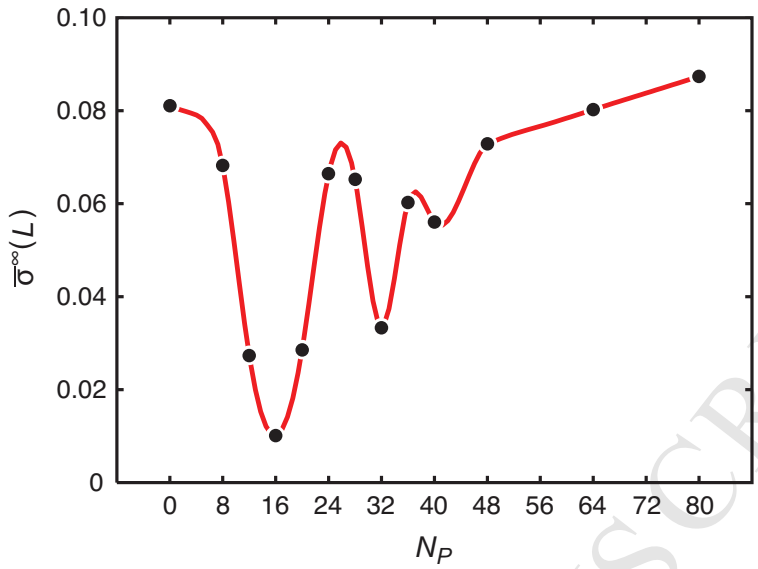

Figure 2: Average value of the normalized standard deviation of the outlet cross-sectional temperature field, $\overline{\sigma}^{\infty}(L)$, under steady-periodic conditions, as a function of N_P for the rotating, eccentric, 3-D annular heat exchanger. The geometric and velocity parameters are $R_2/R_1 = 2$, $\epsilon = 0.5$, $N_T = 30$, $\Omega_1 = \overline{\Omega}_1(1 + 0.9\sin\omega t)$, $\overline{\Omega}_1/\Omega_2 = -2$. Both the axial and cross-sectional Péclet numbers, $\mathrm{Pe}_z = \langle V_z\rangle L/\eta$ and $\mathrm{Pe}_\Omega = |\Omega_2|R_2(R_2 - R_1)/\eta$, are fixed at 5×10^3. The line is a smooth interpolation of the numerical data and serves as a guide to the eye.

---

value $N_T = 30$. Notice that the curve of $\overline{\sigma}^{\infty}(L)$ vs N_P exhibits a value for which the standard deviation is a minimum. Obviously, it is at this modulation frequency that the apparatus must be operated if the heat transfer rate into the fluid is to be a maximum. Above or below the modulation frequency the mixing and heat transfer rates within the cross-section are not as good.

Figure 3 shows color plots of the steady-periodic temperature field for the exit cross section of the heat exchanger for different values of the flow parameters N_T and N_P; for

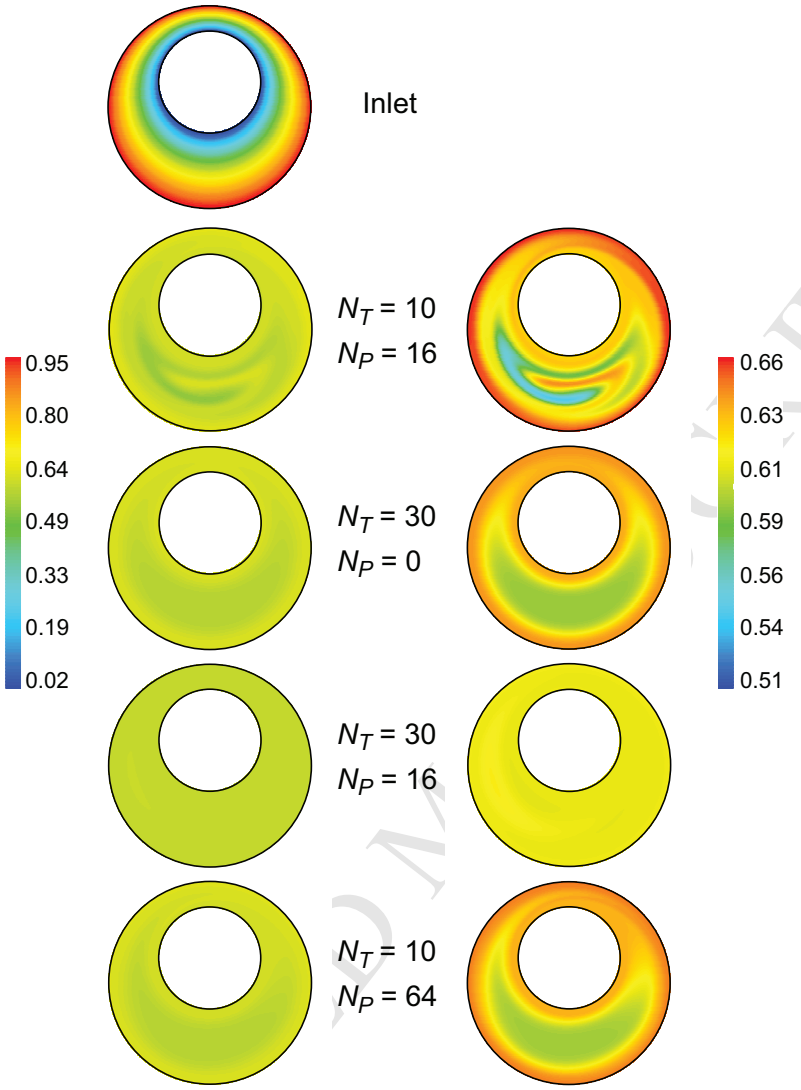

Figure 3: Temperature field for the exit cross section of the heat exchanger as a function of N_P and N_T. The top plot shows the cross-sectional temperature distribution at the inlet of the heat exchanger, as given by Eq. (19). The snapshots of the exit temperature fields were generated under steady-periodic conditions at a time instant that is a multiple of the modulation period ($2\pi/\omega$). The geometry and flow parameters are identical to those of Fig. 2.

reference, the topmost plot shows the inlet temperature distribution, which is the same for all cases, it is defined by Eq. (19). The set of flow parameters considered in Fig. 3 includes the

cases of steady rotation of the inner cylinder ($N_P = 0$), low and moderate angular rotations ($N_T = 10$ and $N_T = 30$), and medium and high forcing frequencies ($N_P = 16$ and $N_P = 64$). The cross-sectional temperature fields in the left-hand column use the same color scale as that for the inlet temperature distribution; the righthand plots employ a color scale that varies over a much smaller temperature range to give a better visualization of the temperature non-uniformities.

Figure 3 shows that a homogeneous outlet temperature field is obtained for the pair of parameter values $\{N_T = 30, N_P = 16\}$. However, it is incorrect to deduce that the value $N_P = 16$ is optimal regardless of the value of N_T, as can be seen by analyzing the first case in Fig. 3. Notice also that the exit temperature field for $\{N_T = 30, N_P = 64\}$ is quite similar to that obtained for steady rotation of the inner cylinder ($N_T = 30, N_P = 0$).

The above results can be confirmed indirectly by other methods based on the analogy between heat and momentum transfer. One tool consists of placing a blob of dye at the flow entrance and then following the trajectory of each individual particle all the way to the exit. The location where each particle crosses the outlet cross section of the heat exchanger is plotted. These calculations are equivalent to solving the 3-D convection-conduction equation, Eq. (18), in a Lagrangian framework for the limiting case of vanishing thermal diffusivity. In this framework, the equations of motion for a non-diffusive scalar are the advection equations,

$$\frac{d\mathbf{x}}{dt} = \mathbf{V}(\mathbf{x}, t), \tag{26}$$

where $\mathbf{x} = (\alpha, \beta, z)$ is the position vector. In the present work, Eq. (26) was integrated over the time coordinate using a fourth-order, semi-implicit Runge-Kutta scheme with error estimation and adaptive stepsize control [18].

Figure 4 shows the outcome of two numerical experiments in which 0.1 vol-% of a passive tracer, consisting of over 10^4 material points, is injected at a specific point of the inlet cross section of the heat exchanger. Two injection locations are considered in Fig. 4: one in the region of maximum gap, the other in the region of minimum clearance. The numerical experiments are performed for a fixed value of $N_T = 30$ and various values of N_P: 0 (no modulation), 16 (optimum frequency), 32 (high frequency), and 64 (very high frequency). Notice how, for the optimum frequency ($N_P = 16$), the tracer spreads over the whole section and much less for the other values of N_P.

In Hamiltonian systems, such as the flow under study but without an axial velocity component (journal bearing flow), the initial location of a tracer particle is important. The revised particle can be introduced either in a poorly mixed region or in a chaotic region. If the particle is introduced outside of a chaotic region it will mix poorly and at the end of each period it will lie somewhere in a well defined domain where there is little stretching. If the particle is placed in a chaotic region, it will spread over a large part of the cross-section and at the end of each period it will be in a new location. A major tool for the study of chaos in 2-D periodic flows is the Poincaré section. It is obtained by tracking a given particle over a very large number of periods.

When an axial Poiseuille velocity profile is superimposed over the above flow, as is the case in the present study, a fluid particle moves forward in the axial direction with an instantaneous velocity that depends on its cross-sectional coordinates. Because of this, a given location can revised be either in a chaotic region or in a regular domain depending on the time instant. While a fluid particle is moved forward by the axial flow inside the heat exchanger, the particle can

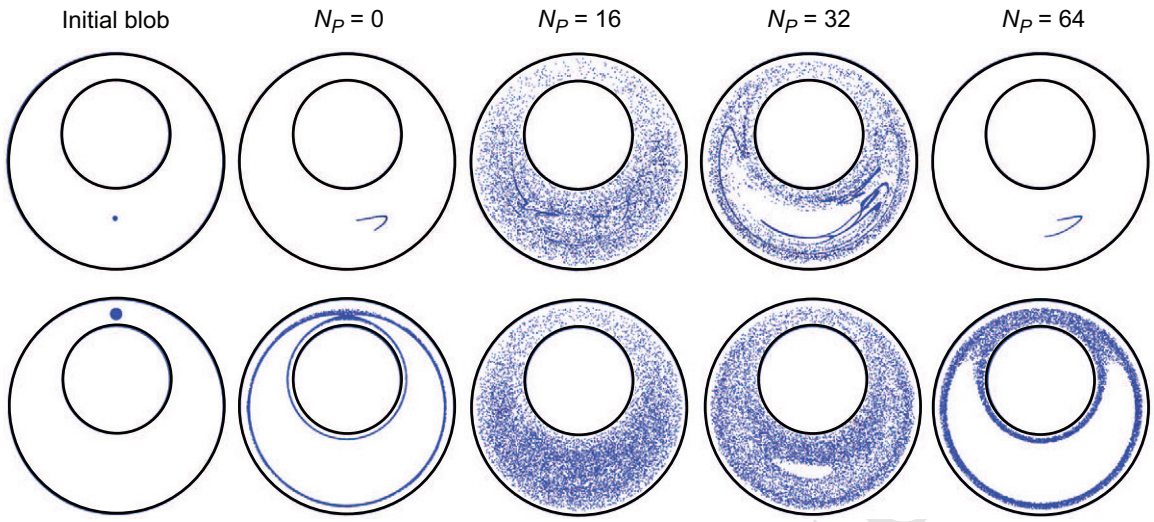

Figure 4: Location of material points at the exit cross section of the heat exchanger for 0.1 vol-% injection of a tracer (passive scalar). The results are presented for different values of N_P and two different injection locations; the exact placements of the injections are shown in the two leftmost plots. The selected values of N_P are: 0 (no modulation), 16 (optimum frequency), 32 (high frequency), and 64 (very high frequency). The geometry and flow parameters are identical to those of Fig. 2. The plots were generated by synchronizing each tracer tracking run with the start of a period of modulation.

find itself in a regular domain for some amount of time, then be trapped in a chaotic region, then escape to another region, and so on. Because of this, the initial location of the particle is more important in the 2-D flow than in its 3-D counterpart.

The initial locations of the two blobs in Fig. 4 are the minimum gap region, where the hyperbolic stagnation point appears in the journal bearing flow (bottom) and the maximum gap region, where the vortex center is placed in the 2-D flow (top). If there was no axial velocity component, only the blob in the hyperbolic point region would mix over a large

part of the cross-section. For the reasons stated above, when the axial velocity component is nonzero, the initial location of the blob is less important even though, qualitatively, the numerical experiments of spreading of a blob show a better mixing when the blob is injected in the narrow gap region.

Another way to highlight the existence of an optimal forcing frequency is to explore the relationship between mixing and stretching in this flow. The computation of stretching, which is related to the increase of interfacial area available for mass and energy transport, was shown to be an alternative route to Poicaré sections and tracer dispersion simulations for characterizing microstructure in chaotic flows [20]. Points experiencing high and low stretching correspond to regions of good and poor micro-mixing, respectively [19, 20]. The rate of stretching determines the rate of the micromixing process both by increasing the intermaterial area over which heat conduction can occur but also by decreasing the required thermal diffusional distance. Stretching calculations are computationally tractable for even 3D flows. This type of calculations was first made in the journal bearing flow by Swanson and Ottino [21].

The stretching vector of a fluid element, $\mathbf{l}$, associated with a tracer particle initially located at $\mathbf{x}_0$ can be calculated by integrating the advection equations, Eq. (26), subject to $(\mathbf{x})_{t=0} = \mathbf{x}_0$, along with

$$\frac{d\mathbf{l}}{dt} = (\nabla \mathbf{V})^T \cdot \mathbf{l}, \quad (\mathbf{l})_{t=0} = \mathbf{l}_0. \tag{27}$$

The total accumulated stretching λ experienced by the fluid element at a given time instant is

$$\lambda = ||\mathbf{l}||/||\mathbf{l}_0||. \tag{28}$$

Stretching calculations were performed with 2×10^4 particles covering uniformly the entrance of the heat exchanger. Each particle was assigned an initial stretch vector $\mathbf{l}_0 = [l_\alpha, l_\beta, l_z] = [0, 0, 1]$. In order to determine the stretching field at the exit of the heat exchanger, the cross section was discretized with a square grid of 100×100 cells. Cells that are entirely within the flow domain were retained, those that fall partially or completely outside the flow domain were discarded. The value of stretching in each cell was approximated as the geometric mean of the stretching values of the tracer particles located within the cell. Since the flow field is time periodic, the overall stretching plot for a given modulation protocol was computed by averaging stretching distributions determined for 10 equally spaced phase angles of the sinusoidal velocity protocol.

Figure 5 shows the time-average stretching field at the exit cross section of the heat exchanger for the same values of the parameters as in Fig. 4. The fluid particles that were subjected to a good stretching rate during their residence in the heat exchanger are colored in white, while regions of poor stretching are colored in blue. One can see in Fig. 5 that the regions of low stretching correspond to the regions in Fig. 3 where the outlet temperature field deviates most from the mean value. Furthermore, there are practically no regions of low stretching rate when the modulation frequency is at its optimum value.

The influence of the eccentricity ratio on the efficiency of the heat exchanger is shown in Fig. 6, where the exit value of the normalized standard deviation of the temperature field, $\overline{\sigma}^{\infty}(L)$, is plotted against N_P for $N_T = 30$ and different values of ϵ. From Fig. 6 it is possible to determine the optimum value of N_P for each value of ϵ; for example, the optimum value for $\epsilon = 0.1$ is $N_P = 12$; over the range $0.3 \leq \epsilon \leq 0.5$ it is $N_P = 16$; for $\epsilon = 0.7$ there are two

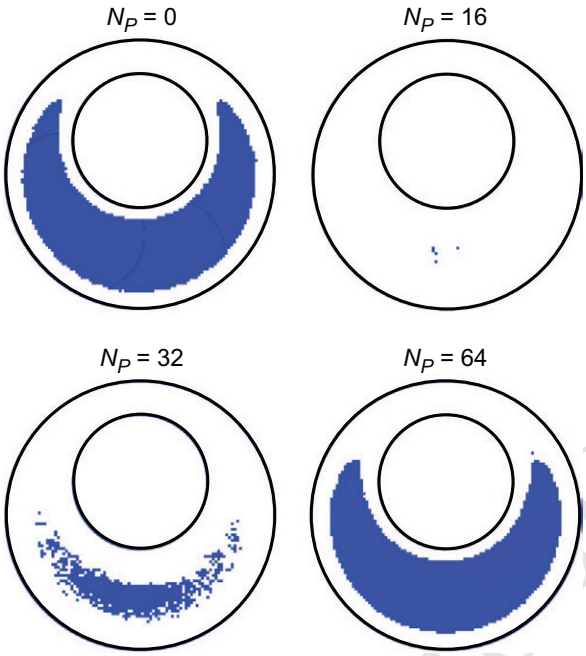

Figure 5: Time averaged stretching field for the exit cross section of the heat exchanger as a function of N_P for a fixed value $N_T = 30$. Any region where the accumulated stretching is less than the cutoff value $\lambda_c = 10^5$ is colored in blue while any region where the stretching is above the cutoff value is white. The geometry and flow parameters are identical to those of Fig. 2.

---

local optimal values of N_P, namely $N_P = 0$ and $N_P = 48$. Notice that the lowest value of the standard deviation is obtained for $\epsilon \approx 0.5$ and $N_P = 16$. It is also for intermediate values of ϵ that the effect of the forcing frequency is more pronounced. For small values of ϵ there is a single local optimum value of N_P. For large values of ϵ, $\overline{\sigma}^{\infty}(L)$ is weakly dependent on N_P.

The color plots of the exit temperature field, displayed in Fig. 7 for selected values of ϵ, show that the best value is actually closer to $\epsilon = 0.4$. These temperature fields were generated at the optimum forcing frequency for each value of ϵ. The thermal profiles can be visually compared in terms of their degree of uniformity or in terms of their degree of

new

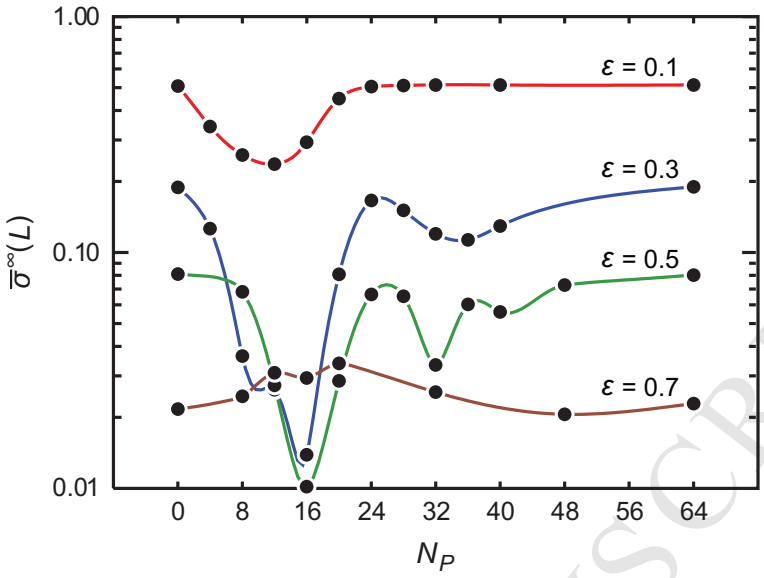

Figure 6: Exit value of the normalized standard deviation of the temperature field, $\overline{\sigma}^{\infty}(L)$, as a function of ϵ and N_P, for the eccentric, rotating, 3-D annular heat exchanger under steady-periodic conditions. The geometric and rotation parameters are the same as in Fig. 2. The lines are a smooth interpolation of the numerical data and serve as guides to the eye.

similitude with the color value of $\langle T \rangle(0)$, which is the exit fluid temperature for a perfectly homogenized heat exchanger. Obviously, both types of comparison yield the same conclusion about the optimal choice of ϵ. Particle tracking in the heat exchanger, Fig. 8, shows that the passive tracer is better and more evenly distributed over the entire exit cross section of the heat exchanger for an eccentricity ratio ϵ between 0.4 and 0.5 and at the same optimum forcing frequency as in Fig. 7.

Chaotic advection in this flow is, perhaps, best visualized by plotting numerical streaklines. As an example, for $\epsilon = 0.5$, $R_2/R_1 = 2$, and $N_T = 30$, Fig. 9 shows the streaklines for the cases of no inner cylinder modulation ($N_P = 0$), optimum modulation ($N_P = 16$), and a very high modulation ($N_P = 64$). The point where the tracer is continuously injected

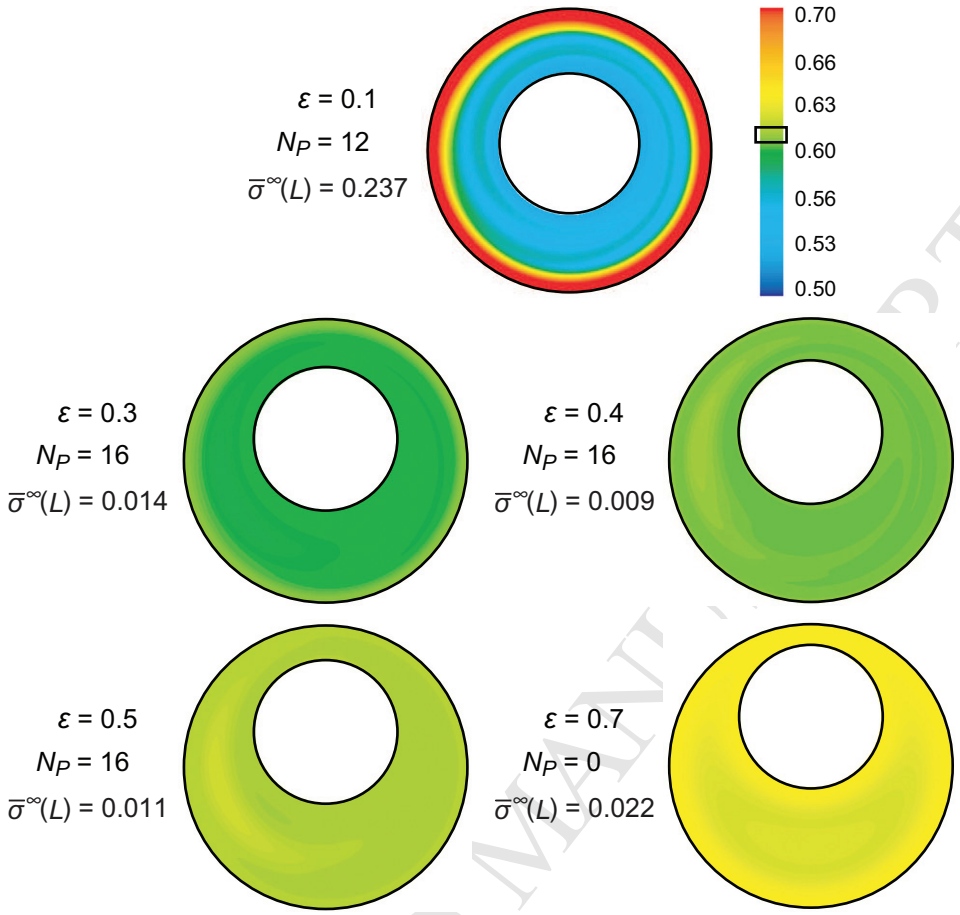

Figure 7: Temperature field at the exit cross section of the heat exchanger as a function of the eccentricity ratio, ϵ, for a fixed value $N_T = 30$ and optimal value of N_P. For each case, the value of the control parameter N_P is the one that minimizes the exit value of the normalized standard deviation of the temperature field, $\overline{\sigma}^{\infty}(L)$ (see Fig. 6). The snapshots of the exit temperature field were generated under steady-periodic conditions at a time instant that is a multiple of the modulation period ($2\pi/\omega$). The geometric and rotation parameters are the same as in Fig. 2. The rectangle over the color scale shows the temperature value if the cross-sectional exit temperature field in the heat exchanger were perfectly homogenized.

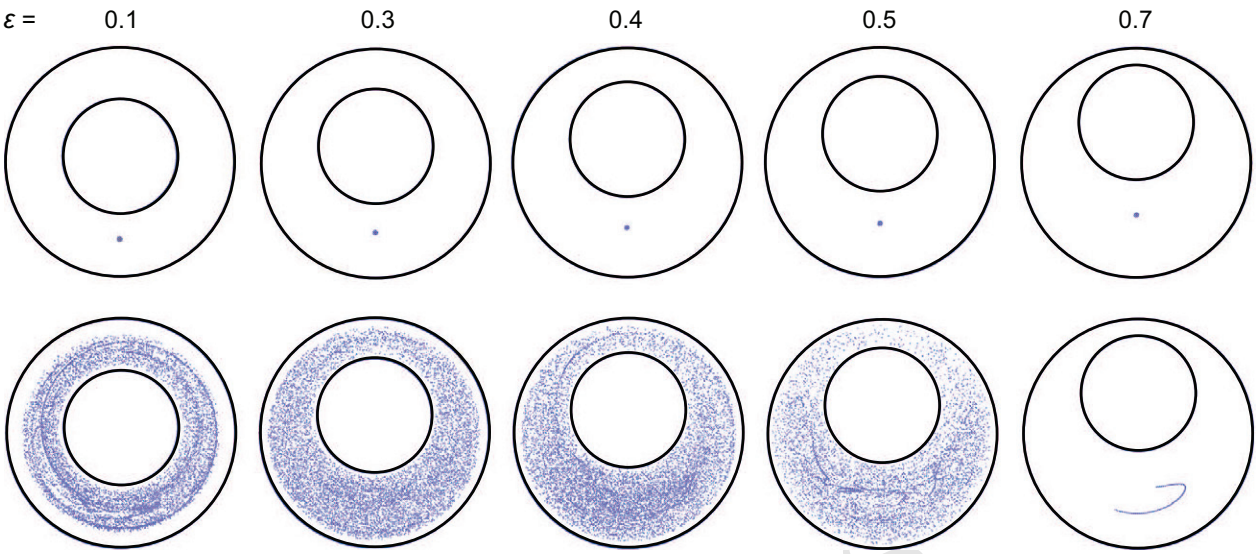

Figure 8: Location of material points at the exit cross section of the heat exchanger for 0.1 vol-% injection of a tracer (passive scalar). The results are presented for different values of ϵ at the optimum forcing frequency for each case. The injection is placed in the region of maximum clearance, its exact placement is shown in the top plots. The values of (ϵ, N_P) are $(0.1, 12)$, $(0.3, 16)$, $(0.4, 16)$, $(0.5, 16)$, and $(0.7, 0)$. The geometry and flow parameters are identical to those of Fig. 2. The plots were generated by synchronizing each tracer tracking run with the start of a period of modulation.

---

is the same in all three cases. When there is no modulation the streaklines are helicoidal, this result is well known and has been shown by Kusch and Ottino [3]. For the optimum modulation frequency, $N_P = 16$, the streaklines are chaotic as shown in middle graphic of Fig. 9. A very high modulation leads to streaklines that are very similar to those obtained without any modulation.

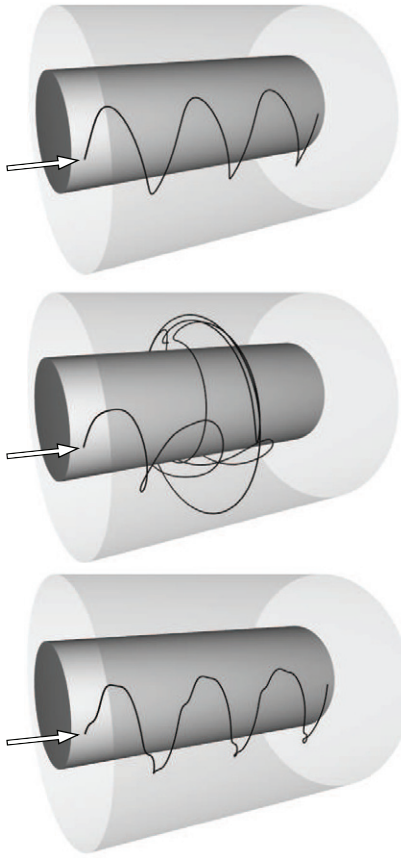

Figure 9: Streaklines for $\epsilon = 0.5$, $R_2/R_1 = 2$, and $N_T = 30$ and three different values of N_P: 0 (top), 16 (middle), and 64 (bottom). The arrows point to the location of the injection point, which is placed in the maximum gap region.

Conclusions

The heat transfer rate into highly viscous, low thermal-conductivity fluids can be enhanced substantially in the eccentric, annular heat exchanger when both boundaries are allowed to rotate. The physical effect of chaotic advection is to render the cross-sectional temperature field uniform, thus increasing both the wall temperature gradient and the heat flux into the fluid. If one boundary moves at constant velocity while the other one turns at a periodic

angular velocity, an optimum forcing frequency exists for which the heat transfer rate is a maximum. The heat transfer efficiency under such conditions is better than that obtained without modulation. The heat transfer enhancement is due to chaotic advection as in turbulent flow. For a given axial flow-rate there is an optimum value of the frequency that enhances the heat-transfer rate most. There is also an optimum value of the eccentricity ratio ϵ. The best performance is obtained for a moderately eccentric heat exchanger, $\epsilon \approx 0.4$–0.5.

Acknowledgements

We thank the anonymous referees for their careful reading and their many suggestions on new improving the presentation of this material. Financial support from the Centre National de la Recherche Scientifique (CNRS) and Requimte/CQFB is gratefully acknowledged.

References

[1] W.M. Kays, Convective Heat and Mass Transfer, McGraw-Hill, New York, 1966.

[2] R.K. Shah, A.L. London, Laminar Flow Forced Convection in Ducts, Academic Press, New York, 1978.

[3] H.A. Kusch, J.M. Ottino, Experiments on mixing in continuous chaotic flows, J. Fluid Mech. 236 (1992) 319–342.

[4] D. V. Khakhar, J.G. Franjione, and J.M. Ottino, A study of chaotic mixing in deterministic flows: the partitioned pipe mixer, Chem. Eng. Sci. 42 (1987) 2909–2926.

[5] D.M. Hobbs, P.D. Swanson, F.J. Muzzio, Numerical characterization of low Reynolds number flow in the Kenics static mixer, Chem. Eng. Sci. 53 (1998) 1565–1584.

[6] G. Metcalfe, D. Lester, Mixing and heat transfer of highly vscous food products with a continuous chaotic flow, J. Food Eng., 95, (2009) 21–29.

[7] G.H. Wannier, A contribution to the hydrodynamics of lubrication, Q. Appl. Math. 8 (1950) 1–32.

[8] R.C. DiPrima, J.T. Stuart, Flow between eccentric rotating cylinders, J. Lub. Tech. Trans. ASME 94 (1972) 266.

[9] B.Y. Ballal, R.S. Rivlin, Flow of a Newtonian fluid between eccentric, rotating cylinders: inertial effects, Arch. Rat. Mech. Anal. 62 (1976) 237–294.

[10] W.T. Snyder, G.A. Goldstein, An analysis of fully developed laminar flow in an eccentric annulus, AIChE J. 11 (1965) 462–467.

[11] S. Ghosh, H.C. Chang, M. Sen, Transport enhancement by steady and time-periodic parallel flow with slender recirculation, J. Fluid Mech., 238, (1992) 119-154.

[12] OpenCFD Ltd., http://www.openfoam.com, 2010.

[13] B.P. Leonard, A stable and accurate convective modeling procedure based on quadratic upstream interpolation, Comput. Meth. Appl. Mech. Eng. 19 (1979), 59-98.

[14] B. van Leer, Towards the ultimate conservative difference scheme. II. Monotonicity and conservation combined in a second order scheme. J. Comp. Phys. 14 (1974) 361–370.

[15] A.J.S. Rodrigo, J.P.B. Mota, A. Lefèvre, E. Saatdjian, On the optimization of mixing protocol in a certain class of three-dimensional Stokes flows, Phys. Fluids 15 (2003) 1505–1516.

[16] A.J.S. Rodrigo, J.P.B. Mota, A. Lefèvre, J.C. Leprévost, E. Saatdjian, Chaotic advection in a 3-D Stokes flow, AIChE J. 49 (2003) 2749–2758.

[17] T.J. Kaper, S. Wiggins, An analytical study of transport in Stokes flows exhibiting large-scale chaos in the eccentric journal bearing, J. Fluid Mech. 253 (1993) 165–174.

[18] P. Kaps, P. Rentrop, Generalized Runge-Kutta methods of order four with stepsize control for stiff ordinary differential equations, Numerische Mathematik 33 (1979) 55–68.

[19] J.M. Ottino, Mixing, chaotic advection and turbulence, Annu. Rev. Fluid Mech. 22 (1990) 207.

[20] F.J. Muzzio, P.D. Swanson, The statistic of stretching and stirring in chaotic flows, Phys. Fluids A 3 (1991) 822.

[21] P.D. Swanson, J.M. Ottino, A comparative computational and experimental study of chaotic mixing of viscous fluids, J. Fluid Mech. 213 (1990) 227–249.